CHEMISTRY OF MATERIALS

pubs.acs.org/cm

Article

Exploration of NaSICON Frameworks as Calcium-Ion Battery Electrodes

Dereje Bekele Tekliye, Ankit Kumar, Xie Weihang, Thelakkattu Devassy Mercy, Pieremanuele Canepa, and Gopalakrishnan Sai Gautam*

Cite This: *Chem. Mater.* 2022, 34, 10133−10143

Read Online

ACCESS | Metrics & More | Article Recommendations | Supporting Information

ABSTRACT: The development of energy storage technologies that are alternative to state-of-the-art lithium-ion batteries but exhibit similar energy densities, lower cost, and better safety is an important step in ensuring a sustainable energy future. Electrochemical systems based on calcium (Ca)-intercalation or deintercalation form such an alternative energy storage technology but require the development of intercalation electrode materials that exhibit reversible Ca-exchange with reasonable energy density and power density performance. To address this issue, we use first-principles calculations to screen over the wide chemical space of sodium superionic conductor (NaSICON) frameworks, with a chemical formula of $Ca_xM_2(ZO_4)_3$ (where M = Ti, V, Cr, Mn, Fe, Co, or Ni and Z = Si, P, or S) for Ca electrode materials. We calculate the average Ca^{2+} intercalation voltage, the thermodynamic stability (at 0 K) of charged and discharged Ca-NaSICON, and the migration barriers of (meta)stable Ca-NaSICON compositions. Importantly, our calculations indicate $Ca_xV_2(PO_4)_3$, $Ca_xMn_2(SO_4)_3$, and $Ca_xFe_2(SO_4)_3$ Ca-NaSICONs to be promising as Ca-cathodes. We find all silicate Ca-NaSICONs to be thermodynamically unstable and hence unsuitable as Ca-cathodes. We report the overall trends in the ground state Ca-vacancy configurations, besides voltages, stabilities, and migration barriers. Our work contributes to unearthing strategies for developing practical calcium-ion batteries, involving polyanionic intercalation frameworks.

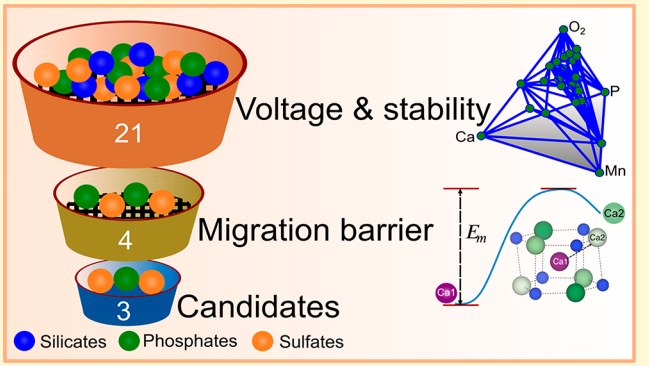

1. INTRODUCTION

Li-ion batteries (LIBs) are well-known for high energy and power density, good cycle life, and reliable performance, making them state-of-the-art in the portable electronics and electric vehicle markets. However, looking into the future, there are various factors with respect to limited availability of lithium (also cobalt and nickel), ever-increasing energy demand, safety concerns, etc., which cast uncertainty over the ability of LIBs to power the world's requirements in the long run.[1−5] Therefore, the advancement and diversification of beyond-lithium (Li) electrochemical energy systems are imperative to fulfill both energy and power demands worldwide. Multivalent batteries, such as those based on magnesium, calcium (Ca), zinc, etc., are an emerging alternative to LIBs because of their high abundance in nature and their use of metal anodes leading to high (volumetric) energy density.[6−11] Among the multivalent systems, calcium is an attractive candidate because of its low standard reduction potential (−2.87 V versus standard hydrogen electrode, SHE) approaching that of Li^+ (−3.04 V versus SHE), low cost, and abundance.[10,12]

The development of Ca-ion batteries (CIBs) or Ca-based electrochemical systems is still in its infancy, especially due to the challenge of finding "compact" cathode materials with high reversible capacity and reasonable rate performance, apart from the challenges associated with electrolyte development.[8,13] Several cathode frameworks have been considered as Ca-cathodes, including 3-D "tunnel" structures, layered and spinel compounds, Chevrel phases, and Prussian blue analogues (PBA), with varying degrees of electrochemical performance.[14−16] Theoretical screening approaches, such as using density functional theory (DFT[17,18]) calculations by Arroyo-de Dompablo and collaborators, have investigated Ca intercalation in a wide range of chemistries,[19−21] such as CaFeSO, CaCoSO, CaNiN, Ca_3MnN_3, $Ca(VO)_2(PO_4)_2$, $Ca_2Fe(Si_2O_7)$, $CaM(P_2O_7)$ (M = V, Cr, Mn, Fe, and Co), $CaV_2(P_2O_7)_2$, and α-$VOPO_4$.[20] The authors identified α-$VOPO_4$ as a promising cathode material due to its maximum theoretical specific capacity of 312 mAh g^{-1}, reasonable activation barrier for Ca

Received: September 15, 2022
Revised: October 26, 2022
Published: November 11, 2022

Downloaded via INDIAN INST OF SCIENCE on December 2, 2022 at 02:48:28 (UTC).
See https://pubs.acs.org/sharingguidelines for options on how to legitimately share published articles.

© 2022 American Chemical Society

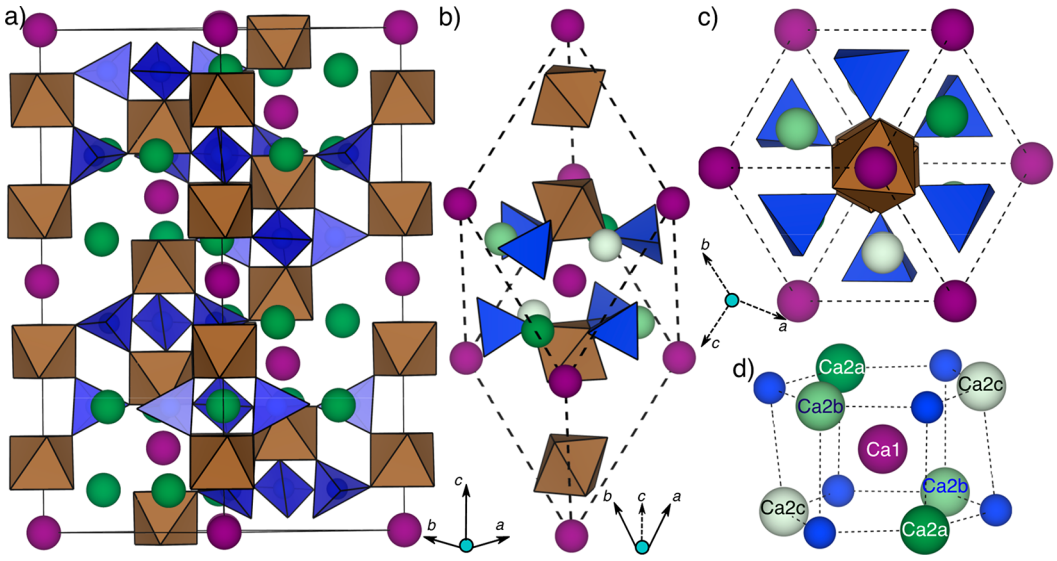

Figure 1. Crystal structures of the NaSICON conventional cell (panel a) and primitive cell (panel b). Brown and blue polyhedra indicate MO_6 and ZO_4 groups, respectively, where oxygen atoms occupy the polyhedral vertices. Purple and dark green spheres in panel (a) indicate Na1 and Na2 sites, respectively, which are equivalent to the Ca1 and Ca2 sites in Ca-NaSICONs. The different shades of green in panels (b), (c), and (d) signify the Ca2a, Ca2b, and Ca2c sites, which together form the Ca2 sites. Dashed black lines indicate the extent of the unit cell. (c) "Top" view of the NaSICON primitive cell, which clearly indicates the rhombohedral symmetry of the underlying structure. (d) A view of the Ca2 and Z sites that neighbor a Ca1 site, forming a hexagonal-prism-like block. Ca migration events in NaSICONs typically occur from a Ca1 site to a neighboring Ca2 site within the hexagonal prism.

diffusion (<0.65 eV), and a robust calculated average voltage of 2.8 V vs Ca. Although $VOPO_4{\cdot}2H_2O$ has shown a reasonable electrochemical performance against Ca-containing electrolytes,[22] given the susceptibility of the framework to undergo proton intercalation,[23] reversible Ca-intercalation in the $VOPO_4$ framework is yet to be rigorously demonstrated.

Several classes of oxide frameworks have been explored as Ca-cathode materials. Liu et al.[14] explored oxide spinels as Ca-cathodes using DFT calculations and found $CaMn_2O_4$ to be a potential cathode with an average intercalation voltage of ∼3.1 V vs Ca and a theoretical gravimetric capacity of 250 mAh g^{-1} with a theoretical energy density of ∼800 Wh/kg. However, the calculated volume change with Ca^{2+} intercalation was found to be >20% which highlighted the instability of the lattice during (de)intercalation of Ca-ions, as later demonstrated by experiments.[24] In the case of (α) δ-V_2O_5, reversible (de)intercalation of Ca has been demonstrated at an average voltage of ∼(3.13) 3.02 V versus Ca^{2+}/Ca, with a theoretical capacity of 242 mAh g^{-1} and activation barrier for Ca mobility of ∼(1700−1900 meV) 200 meV, respectively.[25] However, the experimental investigation by Verrelli et al.[26] elucidated the unsuitability of α-V_2O_5 as an intercalation host for CIB. Because the δ-V_2O_5 is not a stable polymorph, its synthesizability and electrochemical activity remain to be verified by experiment.

Other oxide chemistries that have been investigated as Ca-cathodes include $Ca_4Fe_9O_{17}$ as reported by Black et al., which exhibits a high calculated average voltage of 4.16 V vs Ca, a theoretical capacity of 230 mAh g^{-1}, as well as a reasonable activation barrier for Ca mobility of 0.72 eV.[27] Nonetheless, due to its high voltage, experimental validation of this compound is limited by the electrochemical stability windows of the currently available electrolytes. Recently, Lu et al. reported two promising Ca-cathode compositions, via a DFT-based screening procedure that included average voltages, charge neutrality, thermodynamic stability, and migration barriers, namely, post-spinel-CaV_2O_4 and layered-$CaNb_2O_4$.[28] While recent experiments indicate promise on reversible Ca intercalation in CaV_2O_4, further optimization of the electrode framework is certainly required.[29]

In the chemical space of sulfide cathode materials, Palacín and co-workers have explored the electrochemical activity of Ca in TiS_2 for a variety of electrolytes.[30,31] The authors claimed reversible intercalation (with solvent cointercalation) of Ca in TiS_2 in $Ca(TFSI)_2$:PC electrolyte at 60 °C, 100 °C, and room temperature.[31] Smeu et al. theoretically examined the Chevrel phases of $CaMo_6X_8$ (X = S, Se, Te) as viable Ca-electrodes and found a high activation barrier for Ca mobility in this material (∼780 meV) despite a reasonable intercalation voltage of ∼1.4 V vs Ca^{2+}/Ca.[15] Kuperman et al. investigated the potassium iron hexacyanoferrate (a PBA framework) in a nonaqueous Ca electrolyte and reported reversible capacities of 150 mAh g^{-1} at 23 mA g^{-1} current density.[16] However, the experimental charge/discharge graphs exhibited capacitive-like behavior instead of the desired mechanism of Ca^{2+} intercalation. In the case of the $Ca_{0.89}TaN_2$ framework, Verrelli et al. reported irreversible electrochemical intercalation of Ca.[32] Thus, the search for host materials enabling a reversible Ca-intercalation cathode with reasonable energy density and rate performance is still an active topic of research.

Given the similar size of Ca^{2+} (∼1.00 Å in an octahedral coordination environment surrounded by O^{2-}) compared to Na^+ (∼1.02 Å),[33,34] cathodes that exhibit reversible Na-intercalation may be promising for Ca as well. Sodium superionic conductor (NaSICON) frameworks, which were first reported as Na solid electrolytes by Hong and Goodenough,[35,36] with the classical formula of $Na_{1+x}Zr_2Si_xP_{3-x}O_{12}$ ($0 \le x \le 3$), may be a potential class of tunable polyanionic Ca-cathodes. NaSICON materials comprise a chemical formula $A_xM_2(ZO_4)_3$, where A is the active ion (usually Na^+), M is a transition metal (or a combination of transition metals), and Z is usually Si, P, and/or S (and can also contain

https://doi.org/10.1021/acs.chemmater.2c02841
Chem. Mater. 2022, 34, 10133−10143

elements, such as, Ge, As, etc.).[36] With M being an open-shell transition metal, the NaSICON structure becomes redox-active, and the framework can be a potential electrode material. NaSICON has been explored as a Na-electrode by multiple studies.[37−42] The NaSICON-$NaV_2(PO_4)_3$ framework has been recently shown experimentally to exhibit promising reversible Ca intercalation, with an energy density of ∼220 Wh kg^{-1}, discharge capacity of ∼70 mAh g^{-1}, and average voltage of 3.2 V vs Ca, signifying the promise of NaSICON frameworks as Ca-cathodes.[43]

Structurally, NaSICON contains octahedral MO_6 units (brown polyhedra in the conventional and primitive cells shown in panels (a) and (b) of Figure 1, respectively) connected via corner-sharing ZO_4 tetrahedra (blue polyhedra), forming a three-dimensional skeleton with two distinct intercalant sites, namely, 6-coordinated "Na1" (purple spheres in Figure 1a) and 8-coordinated "Na2" (dark green spheres) sites. Figure 1b shows the primitive cell of the NaSICON which consists of two $M_2(ZO_4)_3$ formula units, while the conventional cell of Figure 1a contains six formula units, with the rhombohedral symmetry of the structure highlighted in the "top" view of Figure 1c. In a Ca-NaSICON, both Na1 and Na2 sites can be occupied by Ca, resulting in "Ca1" and "Ca2" sites, respectively (Figure 1b,d). Note that there is one Ca1 site and three Ca2 sites (labeled as "Ca2a", "Ca2b", and "Ca2c" in Figure 1d) per $M_2(ZO_4)_3$ formula unit. Both Ca1 and Ca2 sites share faces with two MO_6 octahedra, while Ca2 sites also share edges with ZO_4 tetrahedra. Each Ca1 is surrounded by six Ca2 sites and six Z sites in its vicinity, forming a hexagonal-prism-like block, as shown in Figure 1d. Also, the NaSICON framework can be considered to be made of "lantern" units comprising two MO_6 octahedra that are connected by three corner sharing ZO_4 tetrahedra (not shown in Figure 1).[44]

Here, we use DFT-based calculations to screen the chemical space of $Ca_xM_2(ZO_4)_3$, where Z = Si, P, or S and M is a 3*d* transition metal among Ti, V, Cr, Mn, Fe, Co, and Ni, as possible Ca-cathodes. In principle, a $Ca_xM_2(ZO_4)_3$ framework can accommodate an exchange of a maximum of 2 Ca-ions, resulting in an oxidation state change of ±2 per M atom (e.g., $M^{2+} \leftrightarrow M^{4+}$), making Ca-NaSICONs favorable in terms of energy density and motivating our choice of 3*d* transition metals. We calculate the average intercalation voltages, theoretical capacities, thermodynamic stabilities, and migration barriers upon Ca (de)intercalation in the Ca-NaSICON structures and benchmark our results with available experimental data. Specifically, we find $Ca_xV_2(PO_4)_3$, $Ca_xMn_2(SO_4)_3$, and $Ca_xFe_2(SO_4)_3$ to be promising cathode materials in terms of practicable intercalation voltages, thermodynamic (meta)stabilities, and reasonable migration barriers. The high thermodynamic instability eliminates silicate Ca-NaSICONs as Ca-cathode candidates. Ours is a screening study of the diverse chemical space of Ca-NaSICONs as potential calcium intercalation hosts, and we hope that it inspires further theoretical and experimental exploration of NaSICONs as Ca-cathodes.

2. METHODS

All spin-polarized total energy DFT calculations were performed using the Vienna *ab initio* simulation package (VASP),[45,46] by employing the projector-augmented-wave (PAW)[47,48] formalism, where the specific PAW potentials used are identical to those of our previous work[49,50] and listed in the Supporting Information. Expanding the one-electron Kohn−Sham orbitals with a plane-wave kinetic energy cutoff of 520 eV, we employed the Hubbard *U* corrected strongly constrained and appropriately normed (i.e., SCAN+*U*) functional to describe the electronic exchange and correlation.[49−53] The *U* value applied for each transition metal was derived from previous work.[49,50] We utilized Γ-point-centered, Monkhorst−Pack[54] *k*-point meshes with a minimum of 32 subdivisions along each unit reciprocal lattice vector for all structures and a Gaussian smearing (of 0.05 eV) to integrate the Fermi surface. During the structure relaxation, the total energy of each structure was converged within 10^{-5} eV, and the atomic forces were converged to |0.03| eV/Å. Note, we have relaxed the cell volumes, shapes, and ionic positions of all structures without preserving any underlying symmetry in all our calculations.

Given the range of the transition metal oxidation states possible within the NaSICON framework (i.e., $M^{2+} \leftrightarrow M^{4+}$) and assigning oxidation states of +4, +5, and +6 for Si, P, and S, respectively, the Ca-NaSICON structure will remain electrostatically charge neutral for Ca contents in the range of $2 \le x \le 4$ in $Ca_xM_2(SiO_4)_3$, $0.5 \le x \le 2.5$ in $Ca_xM_2(PO_4)_3$, and $0 \le x \le 1$ in $Ca_xM_2(SO_4)_3$. Thus, $Ca_2M_2(SiO_4)_3$, $Ca_{0.5}M_2(PO_4)_3$, and $M_2(SO_4)_3$ constitute "charged" Ca-NaSICON compositions, while $Ca_4M_2(SiO_4)_3$, $Ca_{2.5}M_2(PO_4)_3$, and $Ca_1M_2(SO_4)_3$ correspond to the "discharged" compositions. Among 3*d* transition metals, V can theoretically exhibit a +5 oxidation state. However, the extraction of the final Na in the V-phosphate NaSICON (i.e., Na removal from $NaV_2(PO_4)_3$), which would allow V to exhibit a +5 oxidation state, has not reliably been achieved so far either chemically or electrochemically.[42] Hence, we preclude the possibility of V displaying a +5 oxidation state in $Ca_xV_2(PO_4)_3$. In summary, we assumed a possible exchange of 2 mol of Ca per NaSICON formula unit in silicates and phosphates, besides considering 1 mol of possible Ca exchange per formula unit in sulfates. Note, the theoretical capacities considered in this work should be considered as an upper limit to any experimental measurement.

To generate the initial Ca-NaSICON structures, we used the primitive cell of the $Na_4Zr_2(SiO_4)_3$ framework as the starting guess (2 formula units or 42 atoms), where each 3*d* transition metal substitutes Zr to generate the corresponding Ca-NaSICON framework.[55] The phosphate and sulfate-based Ca-NaSICONs are derived by substituting Si with P and S, respectively. After performing elemental substitutions, the lattice parameters of the theoretically generated Ca-NaSICON structures were scaled using the "RLSVolumePredictor" class of the pymatgen package.[56] All unique Ca-vacancy arrangements in the silicate (i.e., for $Ca_2M_2(SiO_4)_3$), phosphate ($Ca_{0.5}M_2(PO_4)_3$ and $Ca_{2.5}M_2(PO_4)_3$), and sulfate ($Ca_1M_2(SO_4)_3$) NaSICON primitive cells were enumerated using the "enumlib" library by Hart et al.[57−60] In total, we generated 70 $Ca_2M_2(SiO_4)_3$ (10 per transition metal), 14 $Ca_{0.5}M_2(PO_4)_3$, 42 $Ca_{2.5}M_2(PO_4)_3$, and 28 $Ca_1M_2(SO_4)_3$ configurations. The $Ca_4M_2(SiO_4)_3$ and $M_2(SO_4)_3$ compositions comprise one Ca-vacancy configuration per transition metal. Note that all the NaSICON structures considered in this work were generated theoretically, based on the $Na_4Zr_2(SiO_4)_3$ primitive cell.

A reversible intercalation battery based on Ca-NaSICON cathodes involves insertion/extraction of Ca^{2+} into/from the $Ca_xM_2(ZO_4)_3$ framework according to the redox reaction of eq 1.

$$Ca_yM_2(ZO_4)_3 + (x-y)Ca^{2+} + 2(x-y)e^- \leftrightarrow Ca_xM_2(ZO_4)_3 \quad (1)$$

where *y* and *x* are the concentrations of Ca in the charged and discharged Ca-NaSICON structure, respectively. The average intercalation voltage due to (de)intercalation of $(x - y)$ moles of Ca^{2+} can be calculated from the Gibbs energy change, which is approximated by the total energy change as calculated by DFT ($\Delta G \approx \Delta E$, eq 2), ignoring the $p - V$ and entropic contributions.[61] *F* in eq 2 is the Faraday constant, and μ_{Ca} is the Ca chemical potential in pure Ca metal (i.e., in its ground state face-centered-cubic structure).

https://doi.org/10.1021/acs.chemmater.2c02841
Chem. Mater. 2022, 34, 10133−10143

$$\langle V \rangle = -\frac{\Delta G}{2(x-y)F} \approx -\frac{E(Ca_xM_2(ZO_4)_3) - [E(Ca_yM_2(ZO_4)_3) + (x-y)\mu_{Ca}]}{2(x-y)F} \quad (2)$$

To evaluate the thermodynamic stability, we compute the 0 K convex hull of quaternary Ca−M−Z−O systems by considering all possible elements, binaries, ternaries, and quaternaries whose structures are available in the inorganic crystal structure database (ICSD[62]) and calculating their ground state energies with DFT. A list of the binary, ternary, and quaternary compounds calculated by us is provided in the Supporting Information, and the final geometries and energies of all computed structures (except binary transition metal oxides) are also available in the GitHub repository associated with this work.[63] We used the pymatgen[56] package to construct our convex hulls and quantify the extent of instability or stability by calculating the energy above/below the convex hull (E^{hull}).[64] In the case of unstable/metastable phases, (positive) E^{hull} indicates the largest decomposition energy that can be released by the unstable/metastable phase decomposing into its ground state(s). On the other hand, for a stable phase, (negative) E^{hull} is the lowest energy released by the formation of the stable phase from other stable phases within the chemical space.[65] Thus, compounds that are stable have $E^{hull} \leq 0$. Previous studies have used an approximate rule of thumb of $E^{hull} \sim 50$ meV/atom as a threshold of experimental synthesizability,[66] which we also consider here.

We calculated the Ca^{2+} migration barriers (E_m) to investigate Ca-ion mobility within a subset of candidate Ca-NaSICON frameworks, using the DFT-based nudged elastic band (NEB[67]) method. Notably, performing ab initio molecular dynamics simulations for Ca migration can be computationally prohibitive, especially when the migration barriers are high.[68,69] We calculated the E_m at high ("charged" compositions) and/or low ("discharged" compositions) Ca vacancy concentration limits. To set the Ca^{2+} migration path within the framework, we relaxed the initial and final end point configurations, assuming a vacancy-mediated migration mechanism, until the atomic forces were converged to |0.03| eV/Å. We considered all Ca migration events in all Ca-NaSICONs to occur between a Ca1 site and a Ca2 site within the hexagonal-prism displayed in Figure 1d, given previous studies that have established Na migration events to occur between Na1 and Na2 sites in Na-containing NaSICONs.[70,71] The minimum energy path (MEP) was initialized by linearly interpolating the lattice vectors and atomic positions to create seven intermediate images between the end points, with a spring constant of 5 eV per Å between images. The NEB calculation, done on Γ-centered Monkhorst-pack meshes with a density of at least 32 points per Å, was considered converged if the band forces became less than |0.05| eV/Å.

For the NEB calculations, we examined the effect of the choice of the exchange-correlation functional and cell size on E_m by using $Ca_{0.5}V_2(PO_4)_3$ and $Ca_{2.5}V_2(PO_4)_3$ as test cases, with the data presented in Figure S8 and Table S3 of the Supporting Information. Importantly, we found minimal difference in calculated E_m (∼7−13% variation, or ∼80−160 meV) between the Ca-NaSICON primitive cell (2 formula units of $M_2(ZO_4)_3$) and a supercell configuration (8 formula units),[71] thus motivating the use of the primitive cell for further calculations. Note that the distance between migrating Ca^{2+} is >8 Å across its periodic image,[72] which ensures minimal fictitious interactions between the migrating ions. Additionally, we found that the Perdew−Burke−Ernzerhof (PBE[73]) parametrization of the generalized gradient approximation (GGA) consistently provided a lower estimate of E_m (by ∼200 meV) compared to SCAN, consistent with our recent observations across multiple electrode and solid electrolyte materials.[74] Moreover, we found a negligible difference (∼40 meV) in calculated E_m between SCAN and SCAN+U. Given that SCAN NEB calculations are computationally more expensive and are notoriously difficult to converge compared to GGA and that GGA provides reliable qualitative trends on calculated E_m,[74] the E_m data presented here, especially of the promising candidates, is calculated using GGA. All calculated minimum energy pathways, including GGA and SCAN NEBs, are compiled in Figures S9, S10, and S11 of the Supporting Information.

3. RESULTS

3.1. Structural Features of $Ca_xM_2(SiO_4)_3$, $Ca_xM_2(PO_4)_3$, and $Ca_xM_2(SO_4)_3$.

Table 1 lists the ground state Ca-vacancy configurations, in terms of occupancy of each Ca site type, for all charged and discharged Ca-NaSICON compositions considered here. Representations of these configurations and their simulated XRD pattern are shown in Figures S1 and S2−S4 of the Supporting Information, respectively.

Table 1. Site Occupancy of the Ca1, Ca2a, Ca2b, and Ca2c Sites in the Calculated Ground State Configurations for Each Ca-NaSICON Composition Considered[a]

Composition	Ca site occupancy in ground state			
	Ca1	Ca2a	Ca2b	Ca2c
Silicates				
$Ca_4M_2(SiO_4)_3$	1.0	1.0	1.0	1.0
$Ca_2M'_2(SiO_4)_3$, M′ = Ti, V, Cr, Mn, Fe	1.0	1.0	0.0	0.0
$Ca_2Co_2(SiO_4)_3$	0.5	1.0	0.5	0.0
$Ca_2Ni_2(SiO_4)_3$	0.5	0.5	0.5	0.5
Phosphates				
$Ca_{2.5}M_2(PO_4)_3$	1.0	0.5	0.5	0.5
$Ca_{0.5}M_2(PO_4)_3$	0.5	0.0	0.0	0.0
Sulfates				
$Ca_1M_2(SO_4)_3$	1.0	0.0	0.0	0.0
$M_2(SO_4)_3$	0.0	0.0	0.0	0.0

[a]In a Ca-NaSICON primitive cell, there are two Ca sites of each type, indicating that the possible occupancy of each Ca site is 0.0, 0.5, or 1.0. M in the table with all transition metals considered (i.e., Ti, V, Cr, Mn, Fe, Co, and Ni). A schematic of all ground state configurations is provided in Figure S1.

For the discharged ($Ca_{2.5}M_2(PO_4)_3$) and the charged ($Ca_{0.5}M_2(PO_4)_3$) phosphates, the ground state Ca-vacancy configuration is identical for all transition metals within each compositional group. For example, in $Ca_{2.5}M_2(PO_4)_3$, the Ca1 site is fully occupied, and all Ca2 sites display a 0.5 occupancy. In the case of $Ca_{0.5}M_2(PO_4)_3$, the Ca1 site exhibits half occupancy for all transition metals, with all Ca2 sites being fully empty. Similarly, the discharged $Ca_1M_2(SO_4)_3$ shows an identical ground state Ca-vacancy configuration for all transition metals, with the Ca1 site being fully occupied and all Ca2 sites being fully empty. The presence of P^{5+} and S^{6+} in the ZO_4 tetrahedra exert strong electrostatic repulsions on the Ca^{2+}, forcing them to occupy fully the Ca1 sites (which only share corners with ZO_4 tetrahedra) before any of the Ca2 sites are occupied in both phosphates and sulfates.

Discharged silicate compounds, with composition $Ca_4M_2(SiO_4)_3$, involve Ca occupying all four Ca sites fully occupied (Figure S1d). Similar to the phosphates and sulfates, the ground state configuration of the charged compositions of $Ca_2M_2(SiO_4)_3$ for M = Ti, V, Cr, Mn, and Fe (Figure S1a) are identical, with Ca-ions fully occupying the Ca1 and the Ca2a sites. However, the ground state configuration of the charged $Ca_2Co_2(SiO_4)_3$ (Figure S1b) and $Ca_2Ni_2(SiO_4)_3$ (Figure S1c) are distinct from those of the other TM analogues. In the case of $Ca_2Co_2(SiO_4)_3$, the Ca2c site is fully occupied with the Ca1 and Ca2a sites being half occupied. In contrast, all Ca sites are

https://doi.org/10.1021/acs.chemmater.2c02841
Chem. Mater. 2022, 34, 10133−10143

half-occupied in the case of $Ca_2Ni_2(SiO_4)_3$. Note that both Si and the transition metal have a nominal 4+ oxidation state at compositions $Ca_4M_2(SiO_4)_3$, indicating that the occupancy of Ca sites can be influenced by both electrostatic effects as well as the hybridization effects of the $M^{4+}-O^{2-}$ and $Si^{4+}-O^{2-}$ bonds. These effects explain the different occupancies observed in the charged Co- and Ni-silicates.

3.2. Intercalation Voltages and Theoretical Capacities of Ca-NaSICONs. Figure 2 displays a comparison of the computed average voltage (in Volts versus Ca metal), for silicate (blue symbols), phosphate (green), and sulfate (orange) Ca-NaSICONs across the entire range of chemically accessible compositions (i.e., $Ca_2M_2(SiO_4)_3 \leftrightarrow Ca_4M_2(SiO_4)_3$, $Ca_{0.5}M_2(PO_4)_3 \leftrightarrow Ca_{2.5}M_2(PO_4)_3$, and $M_2(SO_4)_3 \leftrightarrow Ca_1M_2(SO_4)_3$) for each 3*d* transition metal considered. We also compile all calculated voltages and the corresponding gravimetric capacities (in mAh g^{-1}) in Table 2. Expectedly, the theoretical capacities that are calculated with reference to the charged compositions decrease from Ti to Ni for silicates (from 237 to 226 mAh g^{-1}, see Table 2), phosphates (268 to 254 mAh g^{-1}), and sulfates (140 to 132 mAh g^{-1}), corresponding to an increase of atomic mass from Ti to Ni.

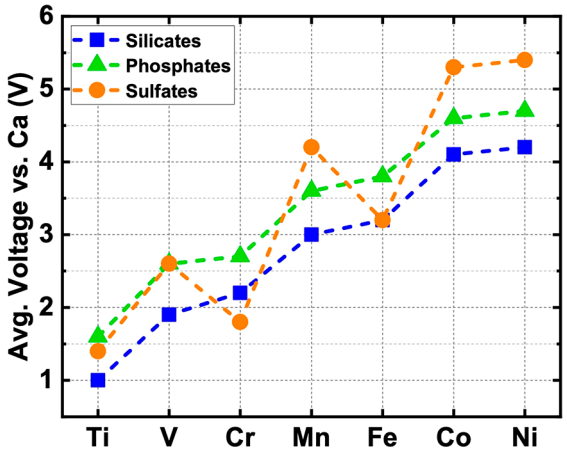

Figure 2. Computed average voltage as a function of transition metal, between the fully discharged and charged Ca-NaSICON compositions for silicate (blue squares), phosphate (green triangles), and sulfate (orange circles) chemistries.

Table 2. Average Intercalation Voltage (in Volts vs Ca) and the Theoretical Capacity (in mAh g^{-1}) of Silicates, Phosphates, and Sulfates-Based Ca-NaSICON Shown for the 3*d* Transition Metals[a]

	Average Voltage (V)			Theoretical Capacity (mAh g^{-1})		
M	Silicate	Phosphate	Sulfate	Silicate	Phosphate	Sulfate
Ti	1.0	1.6	1.4	237	268	140
V	1.9	2.6	2.6	234	264	137
Cr	2.2	2.7	1.8	233	262	137
Mn	3.0	3.6	4.2	230	258	135
Fe	3.2	3.8	3.2	229	257	134
Co	4.1	4.6	5.3	226	254	132
Ni	4.2	4.7	5.4	226	254	132

[a]The theoretical capacities are computed with respect to the molar mass of $Ca_2M_2(SiO_4)_3$ for silicates, $Ca_{0.5}M_2(PO_4)_3$ for phosphates, and $M_2(SO_4)_3$ for sulfates.

Additionally, phosphates and silicates exhibit approximately twice the capacity of sulfates, indicating the possible exchange of two Ca^{2+} in phosphates and silicates compared to one Ca^{2+} in sulfates. Among phosphate and silicate compounds, phosphate NaSICONs exhibit consistently a higher theoretical capacity than silicates owing to the lower mass of the charged composition (i.e., $Ca_{0.5}M_2(PO_4)_3$ vs $Ca_2M_2(SiO_4)_3$).

The predicted average voltages for silicate and phosphate Ca-NaSICONs increase monotonically from Ti to Ni (Figure 2), consistent with trends in the crystal reduction potentials across the +2 ↔ +4 oxidation states of the transition metals.[75] Note that trends in crystal reduction potentials are qualitatively consistent with the standard reduction potentials for several systems.[76] Indeed, the average Ca intercalation voltage raises from ~1.6 V (1.0 V) vs Ca in the Ti-phosphate (silicate) to ~4.7 V (4.2 V) in the Ni-phosphate (silicate). Additionally, the average voltages of the phosphate Ca-NaSICONs are persistently higher than the corresponding silicates for all transition metals, which is expected as a result of the stronger inductive effect exerted by P^{5+} compared to Si^{4+} on the transition metal octahedra.[77,78] For example, the estimated average Ca (de)intercalation voltage in $Ca_xMn_2(PO_4)_3$ is ~3.6 V vs Ca, which is ~0.6 V higher than the corresponding $Ca_xMn_2(SiO_4)_3$. Furthermore, our predicted Ca intercalation voltage in $Ca_xV_2(PO_4)_3$ (~2.6 V) is lower than the experimentally reported ~3.2 V for Ca intercalation in $NaV_2(PO_4)_3$,[43,79] where the difference between theoretical and experimental voltages can be attributed to the presence of the residual Na in the Ca-NaSICON structure. Thus, the phosphate NaSICONs should exhibit higher energy densities compared to the silicate analogues owing to their higher intercalation voltages and marginally superior gravimetric capacities.

In the case of sulfates, the calculated average voltages exhibit a nonmonotonic trend, with Cr and Fe sulfates showing a markedly lower voltage than their adjacent transition metals. Importantly, Mn, Co, and Ni-based sulfates exhibit higher voltages than the corresponding silicates and phosphates. This observation can be partly attributed to the stronger inductive effect of S^{6+} compared to P^{5+} and Si^{4+}.[77,78] V-sulfate and Fe-sulfate Ca-NaSICONs exhibit identical voltages to V-phosphate (~2.6 V) and Fe-silicate (~3.2 V), respectively, highlighting the balancing effect of the inductive effect differences and the oxidation state of the transition metal undergoing redox. Note that higher oxidation states typically result in higher voltages and that all sulfate Ca-NaSICONs involve transition metals undergoing a $M^{3+} \leftrightarrow M^{2+}$ redox (as constrained by charge neutrality) compared to $M^{4+} \leftrightarrow M^{2+}$ in phosphate and silicate Ca-NaSICONs. Also, the high stability of the Cr^{3+} and Fe^{3+} oxidation states, attributed to their high-spin t_{2g}^3 and $t_{2g}^3e_g^2$ electronic configurations, respectively,[80,81] in their corresponding charged sulfate compositions is the primary reason for the local minimum in calculated voltages at Cr and Fe (Figure 2). Furthermore, the lower voltage of Cr sulfate (~1.8 V), compared to the corresponding silicate (~2.2 V) and phosphate (~2.7 V), can also be largely attributed to the stability of Cr^{3+}.

Intuitively, we expect Ti-based Ca-NaSICONs to be candidate materials for Ca-anodes instead of cathodes, owing to their lower voltages across the polyanionic groups (1.0−1.6 V) investigated here. In terms of intercalation voltages alone, Co- and Ni-based Ca-NaSICONs are promising (>4 V across polyanionic systems), but their experimental accessibility given

https://doi.org/10.1021/acs.chemmater.2c02841
Chem. Mater. 2022, 34, 10133−10143

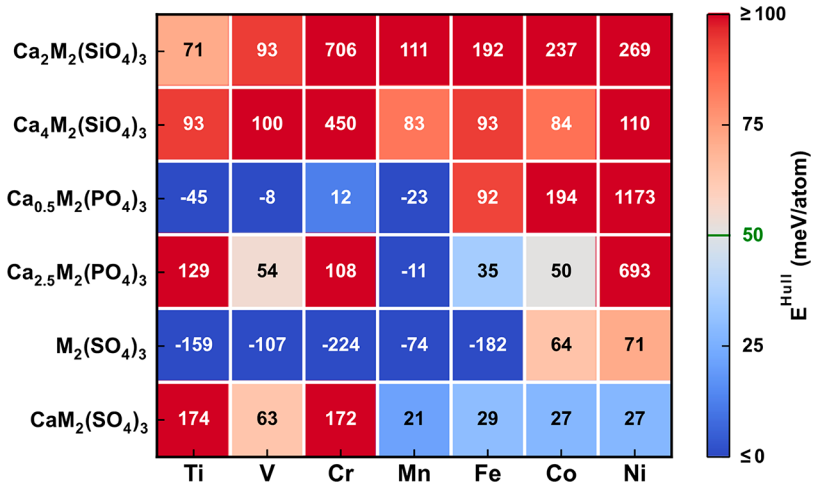

Figure 3. Energy above or below the ground-state convex hull (E^{hull}) extracted from the DFT calculations for charged and discharged silicate (top two rows), phosphate (middle two rows), and sulfate (bottom two rows) Ca-NaSICON. Each column represents a given 3*d* transition metal. Blue (red) squares indicate high degrees of stability (instability), with the specific E^{hull} value of each composition listed as a text annotation in the corresponding square. The green line on the legend bar indicates the rule-of-thumb E^{hull} ~ 50 meV/atom threshold for experimental synthesizability.[66]

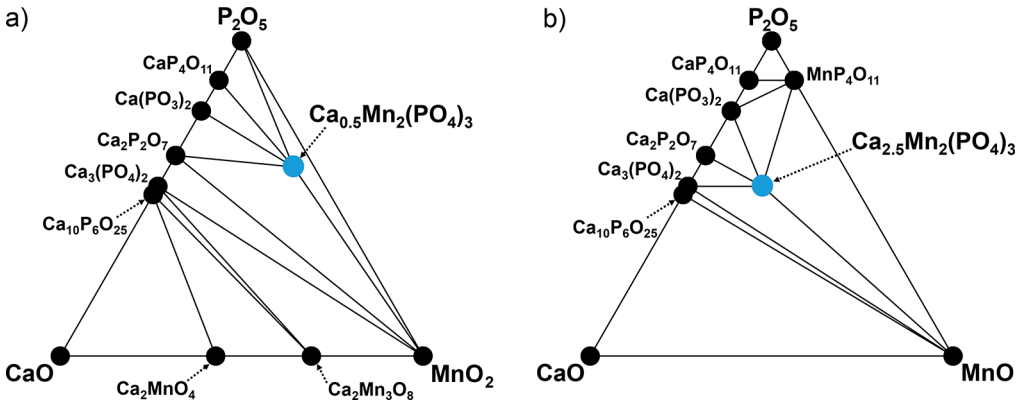

Figure 4. Calculated 0 K Ca−Mn−P−O quaternary phase diagrams showing the charged (panel a) and discharged (panel b) Ca-NaSICON (i.e., $Ca_xMn_2(PO_4)_3$) compositions. For ease of visualization, the pseudoternary projections of the Ca−Mn−P−O chemical space are plotted, namely, $CaO-P_2O_5-MnO_2$ in panel (a) and $CaO-P_2O_5-MnO$ in panel (b). All stable compositions within the phase diagram are indicated by solid black circles, while solid black lines indicate tie-lines. The Ca-NaSICON compositions are indicated by solid light blue circles.

the stability limits[11,82] of current Ca electrolytes is uncertain, while their potential synthesizability is discussed in the following section. With the exception of V- and Cr-silicates (showing average voltages <2.5 V), other V-, Cr-, Mn-, and Fe-systems are candidates exhibiting moderate intercalation voltages (2.5−4.2 V). Combining the average voltages with the theoretical capacities, we observe the phosphate-based Ca-NaSICONs to be more promising than silicates and sulfates in terms of the gravimetric energy density. However, the practical realization of any Ca-NaSICON system as a Ca-cathode clearly depends on its thermodynamic stability and experimental accessibility.

3.3. Thermodynamic Stabilities of Ca-NaSICONs.

Figure 3 depicts the thermodynamic (in)stability of the charged and discharged Ca-NaSICON compositions based on the silicate (top rows), phosphate (middle rows), and sulfate (bottom rows) host chemistry, with each column representing a transition metal. The green line on the legend bar indicates the E^{hull} ~ 50 meV/atom rule-of-thumb synthesizability threshold.[66] Although we use an empirical synthesizability threshold here, the eventual formation, or not, of a metastable compound depends critically upon the thermodynamic behavior of the competing phases. Text annotation in each square indicates the E^{hull} for the corresponding composition. The 0 K convex hulls for the charged and discharged $Ca_xMn_2(PO_4)_3$ NaSICON are depicted in Figure 4, while the convex hulls for the other NaSICONs are compiled in Figures S5−S7 of the Supporting Information. For all unstable (E^{hull} > 50 meV/atom) or metastable (0 < E^{hull} ≤ 50 meV/atom) Ca-NaSICONs, the predicted decomposition products are compiled in Table S1, while for the stable (E^{hull} ≤ 0 meV/atom) Ca-NaSICONs, the "adjacent" phases[65] in their corresponding quaternary phase diagrams are listed in Table S2.

Importantly, for all transition metals considered (both charged and discharged), silicate Ca-NaSICON compositions exhibit a large positive E^{hull} (~71−706 meV/atom), which is beyond the ~50 meV/atom threshold. This indicates their high thermodynamic instabilities. For instance, $Ca_2Mn_2(SiO_4)_3$ (E^{hull} = ~111 meV/atom) is predicted to decompose to other stable phases in the Ca−Mn−Si−O quaternary phase diagram, including $Ca_2Mn_3O_8$, $CaSiO_3$, and SiO_2 (see Figure S5g and

https://doi.org/10.1021/acs.chemmater.2c02841
Chem. Mater. 2022, 34, 10133−10143

Table S1). Thus, we expect all silicate-based Ca-NaSICONs to decompose into other stable phases and thereby are not promising for CIBs.

In the case of phosphates, both charged ($Ca_{0.5}Ni_2(PO_4)_3$, E^{hull} ~ 1173 meV/atom) and discharged ($Ca_{2.5}Ni_2(PO_4)_3$, E^{hull} ~ 693 meV/atom) Ni-NaSICONs show high E^{hull}, clearly indicating the lack of synthesizability of these potential high-voltage phases. Similarly, unstable phosphate Ca-NaSICONs include $Ca_{2.5}Ti_2(PO_4)_3$ (E^{hull} ~ 129 meV/atom), $Ca_{2.5}Cr_2(PO_4)_3$ (108 meV/atom), $Ca_{0.5}Fe_2(PO_4)_3$ (92 meV/atom), and $Ca_{0.5}Co_2(PO_4)_3$ (194 meV/atom), all of which lie above the 50 meV/atom threshold. Notably, the E^{hull} for $Ca_{0.5}Cr_2(PO_4)_3$ (~12 meV/atom), $Ca_{2.5}Fe_2(PO_4)_3$ (~35 meV/atom), and $Ca_{2.5}Co_2(PO_4)_3$ (~50 meV/atom) lie on/below the stabilization threshold, while $Ca_{2.5}V_2(PO_4)_3$ (~54 meV/atom) lies only marginally above the threshold, signifying that these compounds may be obtained experimentally.

We find a set of phosphate and sulfate-based Ca-NaSICONs that are thermodynamically stable. Among the phosphate materials, the stable frameworks include $Ca_{0.5}V_2(PO_4)_3$ (~−8 meV/atom), $Ca_{0.5}Mn_2(PO_4)_3$ (~−23 meV/atom), $Ca_{2.5}Mn_2(PO_4)_3$ (~−11 meV/atom), and $Ca_{0.5}Ti_2(PO_4)_3$ (E^{hull} ~ −45 meV/atom). Note that we depict the pseudoternary projections of the Ca−Mn−P−O chemical space corresponding to the charged $Ca_{0.5}Mn_2(PO_4)_3$ and the discharged $Ca_{2.5}Mn_2(PO_4)_3$ compositions in Figure 4. Ca has been experimentally shown to reversibly intercalate in $NaV_2(PO_4)_3$,[43,79] which is in good agreement with our predictions of $Ca_{0.5}V_2(PO_4)_3$ being thermodynamically stable. Furthermore, the presence of residual Na in $V_2(PO_4)_3$ may stabilize the Ca-NaSICON framework as the Ca concentration increases (i.e., toward the discharged composition), thus promoting electrochemical reversibility. Among sulfate Ca-NaSICONs, we predict all charged compositions, except $Co_2(SO_4)_3$ (E^{hull} ~ 64 meV/atom) and $Ni_2(SO_4)_3$ (~71 meV/atom), to be thermodynamically stable, in agreement with the fact that $Ti_2(SO_4)_3$, $Cr_2(SO_4)_3$, and $Fe_2(SO_4)_3$ are experimentally synthesizeable.[83−85] Additionally, our predictions of a high degree of thermodynamic stability of $V_2(SO_4)_3$ (E^{hull} ~ −107 meV/atom) and $Mn_2(SO_4)_3$ (E^{hull} ~ −74 meV/atom) indicate a promise that these compounds may be synthesized in the future. Several discharged sulfate Ca-NaSICONs that are metastable include $CaMn_2(SO_4)_3$ (~21 meV/atom), $CaFe_2(SO_4)_3$ (~29 meV/atom), $CaCo_2(SO_4)_3$ (~27 meV/atom), and $CaNi_2(SO_4)_3$ (~27 meV/atom).

For practical realization of potential cathodes, both the charged and the discharged phases should be preferably thermodynamically stable to prevent any competing decomposition/conversion reactions[86] from occurring. Under such a constraint, we only find $Ca_xMn_2(PO_4)_3$ (Figure 4) to be a candidate cathode. However, there are known examples of cathodes in other electrochemical systems, where either the charged or the discharged configurations are metastable but exhibit good, reversible performance.[87−90] Thus, if we allow for either the discharged or the charged phase to be stable with the corresponding charged or discharged phase to be metastable, we find Mn- and Fe-sulfate Ca-NaSICONs to be possible candidates, albeit with lower predicted energy densities compared to the Mn-phosphate (Table 2). Given that Ca has been experimentally intercalated into the $NaV_2(PO_4)_3$ structure[43] and given that $Ca_{2.5}V_2(PO_4)_3$ lies only marginally above the 50 meV/atom threshold, we observe the V-phosphate Ca-NaSICON to be a cathode candidate as well. Other materials that may be promising from a purely synthesizability perspective (i.e., $E^{hull} \leq 50$ meV/atom) and not necessarily with cathode applications are $Ca_{2.5}Fe_2(PO_4)_3$, $Ca_{2.5}Co_2(PO_4)_3$, $Ca_{0.5}Ti_2(PO_4)_3$, $Ca_{0.5}Cr_2(PO_4)_3$, $CaCo_2(SO_4)_3$, $CaNi_2(SO_4)_3$, and $V_2(SO_4)_3$.

3.4. Migration Barriers of Ca^{2+} in Ca-NaSICONs. Apart from high intercalation voltage and thermodynamic stability, a Ca-cathode should also exhibit facile Ca^{2+} diffusion to facilitate charge/discharge processes at reasonable rates. The migration of divalent Ca^{2+} in solids is usually poorer than that of monovalent ions (e.g., Li^+, Na^+),[68] typically attributed to Ca^{2+}'s stronger electrostatic interactions leading to local structural distortion during migration of ions. We consider a fairly liberal maximum allowed E_m of ~1000 meV for identifying potential candidates with reasonable rate performance (dashed green line in Figure 5), similar to our previous Ca-cathode screening study.[28]

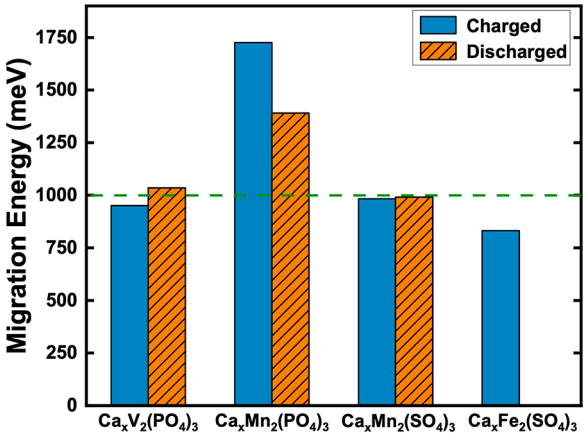

Figure 5. Calculated migration energy barriers of Ca^{2+} in the representative Ca-NaSICON cathode materials, such as $Ca_xV_2(PO_4)_3$, $Ca_xMn_2(PO_4)_3$, $Ca_xMn_2(SO_4)_3$, and $Ca_xFe_2(SO_4)_3$. The solid light blue and hatched orange bar indicate the Ca^{2+} migration energy barriers of the charged and discharged compositions. The horizontal dashed green line indicates the maximum tolerance of the migration energy barrier (E_m = 1000 meV) for a facile migration of Ca-ion in a given anion framework.[28] The minimum energy pathways of Ca^{2+} migration are shown in Figure S9.

The GGA-calculated E_m for the candidate materials, as identified by our voltage and stability calculations, namely, $Ca_xV_2(PO_4)_3$, $Ca_xMn_2(PO_4)_3$, $Ca_xMn_2(SO_4)_3$, and $Ca_xFe_2(SO_4)_3$, are displayed in Figure 5. The E_m values charged and discharged Ca-NaSICON compositions are represented by the light solid blue and hatched orange bars of Figure 5. Despite multiple restarts, the GGA-NEB calculation did not converge for the case of $CaFe_2(SO_4)_3$, explaining the lack of data for the discharged Fe-sulfate Ca-NaSICON. Apart from the candidate Ca-NaSICONs, we have also evaluated E_m for Ca^{2+} migration in a wider set of metastable Ca-NaSICONs using SCAN, including $Ca_{0.5}Cr_2(PO_4)_3$, $Ca_{0.5}Fe_2(PO_4)_3$, $Ca_{0.5}Co_2(PO_4)_3$, $Ca_{2.5}Co_2(PO_4)_3$, $V_2(SO_4)_3$, $CaV_2(SO_4)_3$, $CaCr_2(SO_4)_3$, $Co_2(SO_4)_3$, $CaCo_2(SO_4)_3$, $Ni_2(SO_4)_3$, and $CaNi_2(SO_4)_3$, which is compiled in Figure S11.

Importantly, we find that the E_m of Ca^{2+} in charged V-phosphate Ca-NaSICON (~951 meV) is within the maximum tolerable E_m of ~1000 meV, while the discharged phase (E_m ~ 1035 meV) lies marginally above the tolerance limit. This is in

https://doi.org/10.1021/acs.chemmater.2c02841
Chem. Mater. 2022, 34, 10133−10143

qualitative agreement with the experimental demonstration of Ca (de)intercalation in $NaV_2(PO_4)_3$.[43] Despite the similarity of the ionic size between Ca^{2+} and Na^+ in an octahedral coordination environment and the migration pathways occurring across similar sites (Na1 to Na2 or Ca1 to Ca2), the $Ca^{2+}E_m$ is higher than that of Na^+ in the NaSICON frameworks. This can be attributed to the stability of Ca in the octahedral Ca1 (or Na1) site compared to Na. For example, Jeon et al. recently elucidated that, upon reversible Ca (de)intercalation in $NaV_2(PO_4)_3$, Ca preferably occupies the Na1 (or the Ca1) site by displacing the Na atoms during charge and discharge processes, signifying higher stability of Ca compared to Na at the Na1 (or the Ca1) site.[79] Thus, we believe that the higher migration barrier of Ca^{2+} in NaSICON frameworks is primarily due to the stability of Ca in Ca1 sites rather than any significant variations in the migration pathway itself.

In the case of $Ca_xMn_2(PO_4)_3$, the calculated E_m values in both the charged ($Ca_{0.5}Mn_2(PO_4)_3$, ~1726 meV) and discharged ($Ca_{2.5}Mn_2(PO_4)_3$, ~1391 meV) Mn-phosphate are well beyond the ~1000 meV feasibility limit. We do not expect $Ca_xMn_2(PO_4)_3$ to be a feasible Ca-cathode despite its attractive intercalation voltage and thermodynamic stability. The E_m values of both the charged and the discharged phases of $Ca_xMn_2(SO_4)_3$ (~983 meV and ~991 meV, respectively) and $Ca_xFe_2(SO_4)_3$ (~832 meV) lie below the ~1000 meV tolerance limit, signifying reasonable Ca-ion migration within these frameworks. In summary, we identify $Ca_xV_2(PO_4)_3$, $Ca_xMn_2(SO_4)_3$, and $Ca_xFe_2(SO_4)_3$ as potentially feasible Ca-cathode materials, given their intercalation voltage, thermodynamic (meta)stability, and accessible $Ca^{2+}E_m$.

4. DISCUSSION

Using DFT calculations, we have explored the Ca-NaSICON frameworks as potential cathode materials for CIBs, which are an important technological alternative to current state-of-the-art LIBs. Specifically, we have evaluated the average Ca intercalation voltage, the theoretical capacity, and the 0 K thermodynamic stability for $Ca_xM_2(ZO_4)_3$ systems, where M is a 3*d* transition metal except Sc, Cu, and Zn, Z is either Si, P, or S, and *x* is determined by the overall charge neutrality of the Ca-NaSICON framework. Our calculated data indicates that V-phosphate, Mn- and Fe-sulfate Ca-NaSICONs are promising as Ca-cathodes, among the 21 NaSICON compositions considered, with the overall screening process shown in Figure 6.

In this work, we have used the SCAN+*U* calculations for both our voltage and stability predictions, while GGA was used to calculate the migration barriers. A recent assessment[95] has shown that SCAN+*U* functional exhibits good qualitative trends but tends to overestimate voltages and instabilities in Li-intercalation electrodes. We expect similar trends to be extended to Ca-NaSICONs as well, which is one of the reasons that we used a higher E^{hull} stabilization threshold (~50 meV/atom) than in previous studies (~25 meV/atom).[25,89] However, we expect SCAN+*U*'s trends of high instabilities in silicate-NaSICON frameworks to be a fair evaluation of the Ca−M−Si−O chemical space.

Our calculated 0 K stability data indicates a high degree of instability ($E^{hull} \gg 50$ meV/atom), at both the charged and discharged states, for silicate Ca-NaSICONs. For example, $Ca_2Mn_2(SiO_4)_3$ and $Ca_4Mn_2(SiO_4)_3$ exhibit $E^{hull} \sim 111$ meV/atom and ~83 meV/atom and are expected to decompose into

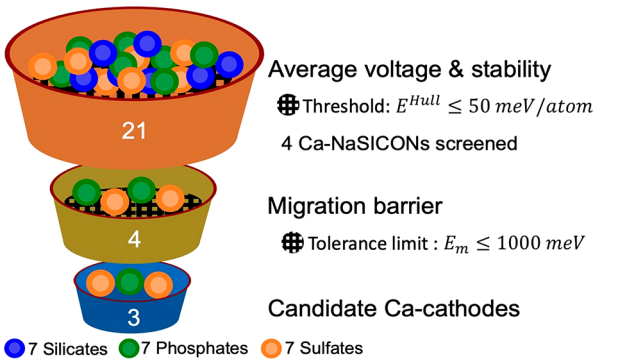

Figure 6. Summary plot depicting the screening process of NaSICON frameworks as Ca-cathodes based on calculated average voltage, thermodynamic stability, and migration barrier. The blue, green, and orange spheres represent silicate, phosphate, and sulfate-based Ca-NaSICONs, respectively. The mesh in the funnel plot represents the threshold for experimental synthesizability ($E^{Hull} \leq 50$ meV/atom) and the maximum tolerance of the migration barrier ($E_m \leq 1000$ meV), resulting in our three candidate compositions, $Ca_xV_2(PO_4)_3$, $Ca_xMn_2(SO_4)_3$, and $Ca_xFe_2(SO_4)_3$.

$Ca_2Mn_3O_8$, $CaSiO_3$, and SiO_2 and $Mn_5Si_3O_{12}$, Ca_2SiO_4, and Mn, respectively (Table S1). Such high instabilities among silicate-NaSICONs are driven largely by the high thermodynamic stability of competing ternary Ca−Si−O compounds, such as $CaSiO_3$, Ca_2SiO_4, $Ca_3Si_2O_7$, and Ca_3SiO, several of which are naturally occurring minerals.[96] Indeed, the E^{hull} of $Ca_2Mn_2(SiO_4)_3$ and $Ca_4Mn_2(SiO_4)_3$ reduce to ~98 meV/atom and ~24 meV/atom, respectively, if all calcium silicate phases are removed from the Ca−Mn−Si−O quaternary phase diagram. In the case of phosphates and sulfates, the number of thermodynamically stable Ca−P−O ($Ca_3(PO_4)_2$) and Ca−S−O ($CaSO_4$) are fewer, thereby driving the instability/metastability of the corresponding Ca-NaSICON compositions to a lower extent compared to the silicates. On one hand, in the search for new Ca-intercalation frameworks, especially with polyanionic materials, chemical spaces containing several known Ca-containing ternary compounds may be avoided. On the other hand, given the diverse chemical space of NaSICON frameworks, tremendous efforts have been made by exploring several transition metal combinations for Na-ion battery cathodes.[37,91−94] Apart from the identified candidate Ca-cathodes in this work, exploring combinations of transition metals within a single Ca-NaSICON framework thus represents a promising strategy for identifying potentially better Ca-cathodes.

5. CONCLUSIONS

Designing cathode intercalation hosts that can reversibly exchange Ca is an important requirement in developing CIBs, as an alternative for the state-of-the-art LIBs. Using first-principles calculations, we explored the Ca-NaSICON frameworks that classically act as Na intercalation frameworks, as potential cathode materials for CIBs. We evaluated the theoretical energy density (i.e., the average Ca intercalation voltage and the theoretical capacity), the 0 K thermodynamic stability for 21 different $Ca_xM_2(ZO_4)_3$ systems, where M = Ti, V, Cr, Mn, Fe, Co, or Ni and Z = Si, P, or S, and the Ca^{2+} migration barriers in select Ca-NaSICON frameworks. The calcium content (*x* in $Ca_xM_2(ZO_4)_3$) was determined by the overall charge neutrality of the Ca-NaSICON framework, for a possible range of $M^{4+} \leftrightarrow M^{2+}$ oxidation states, giving rise to

https://doi.org/10.1021/acs.chemmater.2c02841
Chem. Mater. 2022, 34, 10133−10143

charged compositions of $Ca_2M_2(SiO_4)_3$, $Ca_{0.5}M_2(PO_4)_3$, and $M_2(SO_4)_3$ and discharged compositions of $Ca_4M_2(SiO_4)_3$, $Ca_{2.5}M_2(PO_4)_3$, and $CaM_2(SO_4)_3$ across all transition metals.

We find a monotonic increase in the calculated average voltages for silicates and phosphates through the 3*d* series (i.e., from Ti to Ni), while sulfate Ca-NaSICONs show local minima in calculated voltages at Cr and Fe, attributed to the stability of the Cr^{3+} and Fe^{3+} states. In terms of capacities, we observe phosphates (sulfates) consistently exhibiting the highest (lowest) capacity for all transition metals primarily due to the possibility of two (one) Ca exchange. In terms of thermodynamic stability, we find none of the silicate frameworks to be below our E^{hull} = 50 meV/atom threshold, while several phosphate and sulfate Ca-NaSICONs are either stable or metastable. Combining our calculated voltage, capacity, thermodynamic stability, and migration barrier data, we find the $Ca_xV_2(PO_4)_3$, $Ca_xMn_2(SO_4)_3$, and $Ca_xFe_2(SO_4)_3$ to be promising candidate cathodes for CIBs. We hope that our work inspires further theoretical and experimental studies into Ca-intercalation frameworks, particularly within the chemically diverse Ca-NaSICON space, and drive the practical realization of CIBs.

■ ASSOCIATED CONTENT

Data Availability Statement

All the computational data presented in this study will be made freely available to all on our GitHub repository (https://github.com/sai-mat-group/ca-nasicon-electrodes).

Supporting Information

The Supporting Information is available free of charge at https://pubs.acs.org/doi/10.1021/acs.chemmater.2c02841.

PAW potentials used, schematics of Ca-vacancy configurations of all Ca-NaSICONs considered, pictorial representations of all computed convex hulls at 0 K, list of decomposition products of unstable/metastable Ca-NaSICONs and adjacent phases of stable Ca-NaSICONs, and the migration barriers data (PDF)

■ AUTHOR INFORMATION

Corresponding Author

Gopalakrishnan Sai Gautam − *Department of Materials Engineering, Indian Institute of Science, Bengaluru 560012 Karnataka, India;* orcid.org/0000-0002-1303-0976; Email: saigautamg@iisc.ac.in

Authors

Dereje Bekele Tekliye − *Department of Materials Engineering, Indian Institute of Science, Bengaluru 560012 Karnataka, India*

Ankit Kumar − *Department of Materials Engineering, Indian Institute of Science, Bengaluru 560012 Karnataka, India*

Xie Weihang − *Department of Materials Science and Engineering, National University of Singapore, Singapore 117575, Singapore;* orcid.org/0000-0002-6498-2328

Thelakkattu Devassy Mercy − *Vikram Sarabhai Space Centre, Thiruvananthapuram 695022 Kerala, India*

Pieremanuele Canepa − *Department of Materials Science and Engineering and Department of Chemical and Biomolecular Engineering, National University of Singapore, Singapore 117575, Singapore;* orcid.org/0000-0002-5168-9253

Complete contact information is available at: https://pubs.acs.org/10.1021/acs.chemmater.2c02841

Notes

The authors declare no competing financial interest.

■ ACKNOWLEDGMENTS

G.S.G. acknowledges financial support from the Indian Institute of Science (IISc) Seed Grant (under grant heads SG/MHRD/20/0020 and SR/MHRD/20/0013) and the IISc-Institute of Eminence Travel Grant IE/RERE/22/0501. G.S.G. and A.K. are thankful to the Indian Space Research Organisation-Space Technology Cell for financial support, under sanction number ISTC/MET/SGG/451. D.B.T. thanks IISc for financial assistance. X.W. and P.C. acknowledge funding from the National Research Foundation under the NRF Fellowship NRFF12-2020-0012. P.C. acknowledges support from the Singapore Ministry of Education Academic Fund Tier 1 (R-284-000-186-133). D.B.T., A.K., and G.S.G. acknowledge the computational resources provided by the Supercomputer Education and Research Centre, IISc, for enabling some of the density functional theory calculations showcased in this work. A significant portion of the computational work of this article was performed on resources of the National Supercomputing Centre, Singapore (https://www.nscc.sg).

■ REFERENCES

(1) Whittingham, M. S. Ultimate Limits to Intercalation Reactions for Lithium Batteries. *Chem. Rev.* **2014**, *114* (23), 11414−11443.

(2) Larcher, D.; Tarascon, J.-M. Towards Greener and More Sustainable Batteries for Electrical Energy Storage. *Nat. Chem.* **2015**, *7* (1), 19−29.

(3) Nykvist, B.; Nilsson, M. Rapidly Falling Costs of Battery Packs for Electric Vehicles. *Nat. Clim. Change* **2015**, *5* (4), 329−332.

(4) Tarascon, J.-M. Is Lithium the New Gold? *Nat. Chem.* **2010**, *2* (6), 510−510.

(5) Cano, Z. P.; Banham, D.; Ye, S.; Hintennach, A.; Lu, J.; Fowler, M.; Chen, Z. Batteries and Fuel Cells for Emerging Electric Vehicle Markets. *Nat. Energy* **2018**, *3* (4), 279−289.

(6) Canepa, P.; Sai Gautam, G.; Hannah, D. C.; Malik, R.; Liu, M.; Gallagher, K. G.; Persson, K. A.; Ceder, G. Odyssey of Multivalent Cathode Materials: Open Questions and Future Challenges. *Chem. Rev.* **2017**, *117* (5), 4287−4341.

(7) Ponrouch, A.; Bitenc, J.; Dominko, R.; Lindahl, N.; Johansson, P.; Palacin, M. R. Multivalent Rechargeable Batteries. *Energy Storage Mater.* **2019**, *20*, 253−262.

(8) Arroyo-de Dompablo, M. E.; Ponrouch, A.; Johansson, P.; Palacín, M. R. Achievements, Challenges, and Prospects of Calcium Batteries. *Chem. Rev.* **2020**, *120* (14), 6331−6357.

(9) Blanc, L. E.; Kundu, D.; Nazar, L. F. Scientific Challenges for the Implementation of Zn-Ion Batteries. *Joule* **2020**, *4* (4), 771−799.

(10) Muldoon, J.; Bucur, C. B.; Gregory, T. Quest for Nonaqueous Multivalent Secondary Batteries: Magnesium and Beyond. *Chem. Rev.* **2014**, *114* (23), 11683−11720.

(11) Ponrouch, A.; Frontera, C.; Bardé, F.; Palacín, M. R. Towards a Calcium-Based Rechargeable Battery. *Nat. Mater.* **2016**, *15* (2), 169−172.

(12) El Kharbachi, A.; Zavorotynska, O.; Latroche, M.; Cuevas, F.; Yartys, V.; Fichtner, M. Exploits, Advances and Challenges Benefiting beyond Li-Ion Battery Technologies. *J. Alloys Compd.* **2020**, *817*, 153261.

(13) Monti, D.; Ponrouch, A.; Araujo, R. B.; Barde, F.; Johansson, P.; Palacín, M. R. Multivalent Batteries—Prospects for High Energy Density: Ca Batteries. *Front. Chem.* **2019**, DOI: 10.3389/fchem.2019.00079.

(14) Liu, M.; Rong, Z.; Malik, R.; Canepa, P.; Jain, A.; Ceder, G.; Persson, K. A. Spinel Compounds as Multivalent Battery Cathodes: A

Systematic Evaluation Based on Ab Initio Calculations. *Energy Environ. Sci.* **2015**, *8* (3), 964−974.
(15) Smeu, M.; Hossain, M. S.; Wang, Z.; Timoshevskii, V.; Bevan, K. H.; Zaghib, K. Theoretical Investigation of Chevrel Phase Materials for Cathodes Accommodating Ca^{2+} Ions. *J. Power Sources* **2016**, *306*, 431−436.
(16) Kuperman, N.; Padigi, P.; Goncher, G.; Evans, D.; Thiebes, J.; Solanki, R. High Performance Prussian Blue Cathode for Nonaqueous Ca-Ion Intercalation Battery. *J. Power Sources* **2017**, *342*, 414−418.
(17) Hohenberg, P.; Kohn, W. Inhomogeneous Electron Gas. *Phys. Rev.* **1964**, *136* (3B), B864−B871.
(18) Kohn, W.; Sham, L. J. Self-Consistent Equations Including Exchange and Correlation Effects. *Phys. Rev.* **1965**, *140* (4A), A1133−A1138.
(19) Torres, A.; Bardé, F.; Arroyo-de Dompablo, M. E. Evaluation of Cobalt Oxides for Calcium Battery Cathode Applications. *Solid State Ion.* **2019**, *340*, 115004.
(20) Torres, A.; Casals, J. L.; Arroyo-de Dompablo, M. E. Enlisting Potential Cathode Materials for Rechargeable Ca Batteries. *Chem. Mater.* **2021**, *33* (7), 2488−2497.
(21) Arroyo-de Dompablo, M. E.; Krich, C.; Nava-Avendaño, J.; Palacín, M. R.; Bardé, F. In Quest of Cathode Materials for Ca Ion Batteries: The $CaMO_3$ Perovskites (M = Mo, Cr, Mn, Fe, Co, and Ni). *Phys. Chem. Chem. Phys.* **2016**, *18* (29), 19966−19972.
(22) Wang, J.; Tan, S.; Xiong, F.; Yu, R.; Wu, P.; Cui, L.; An, Q. $VOPO_4{\cdot}2H_2O$ as a New Cathode Material for Rechargeable Ca-Ion Batteries. *Chem. Commun.* **2020**, *56* (26), 3805−3808.
(23) Zima, V.; Beneš, L.; Votinský, J.; Kalousová, J. Intercalation of $VOPO_4{\cdot}2H_2O$ with Hydronium and Potassium Ions. *Solid State Ion.* **1995**, *82* (1), 33−38.
(24) Dompablo, M. E. A.; Krich, C.; Nava-Avendaño, J.; Biškup, N.; Palacín, M. R.; Bardé, F. A Joint Computational and Experimental Evaluation of $CaMn_2O_4$ Polymorphs as Cathode Materials for Ca Ion Batteries. *Chem. Mater.* **2016**, *28* (19), 6886−6893.
(25) Gautam, G. S.; Canepa, P.; Malik, R.; Liu, M.; Persson, K.; Ceder, G. First-Principles Evaluation of Multi-Valent Cation Insertion into Orthorhombic V_2O_5. *Chem. Commun.* **2015**, *51* (71), 13619−13622.
(26) Verrelli, R.; Black, A. P.; Pattanathummasid, C.; Tchitchekova, D. S.; Ponrouch, A.; Oró-Solé, J.; Frontera, C.; Bardé, F.; Rozier, P.; Palacín, M. R. On the Strange Case of Divalent Ions Intercalation in V_2O_5. *J. Power Sources* **2018**, *407*, 162−172.
(27) Black, A. P.; Torres, A.; Frontera, C.; Palacín, M. R.; Arroyo-de Dompablo, M. E. Appraisal of Calcium Ferrites as Cathodes for Calcium Rechargeable Batteries: DFT, Synthesis, Characterization and Electrochemistry of $Ca_4Fe_9O_{17}$. *Dalton Trans.* **2020**, *49* (8), 2671−2679.
(28) Lu, W.; Wang, J.; Sai Gautam, G.; Canepa, P. Searching Ternary Oxides and Chalcogenides as Positive Electrodes for Calcium Batteries. *Chem. Mater.* **2021**, *33* (14), 5809−5821.
(29) Black, A. P.; Frontera, C.; Torres, A.; Recio-Poo, M.; Rozier, P.; Forero-Saboya, J. D.; Fauth, F.; Urones-Garrote, E.; Arroyo-de Dompablo, M. E.; Palacín, M. R. Elucidation of the Redox Activity of $Ca_2MnO_{3.5}$ and CaV_2O_4 in Calcium Batteries Using Operando XRD: Charge Compensation Mechanism and Reversibility. *Energy Storage Mater.* **2022**, *47*, 354−364.
(30) Tchitchekova, D. S.; Ponrouch, A.; Verrelli, R.; Broux, T.; Frontera, C.; Sorrentino, A.; Bardé, F.; Biskup, N.; Arroyo-de Dompablo, M. E.; Palacín, M. R. Electrochemical Intercalation of Calcium and Magnesium in TiS_2: Fundamental Studies Related to Multivalent Battery Applications. *Chem. Mater.* **2018**, *30* (3), 847−856.
(31) Verrelli, R.; Black, A.; Dugas, R.; Tchitchekova, D.; Ponrouch, A.; Palacin, M. R. Steps Towards the Use of TiS_2 Electrodes in Ca Batteries. *J. Electrochem. Soc.* **2020**, *167* (7), 070532.
(32) Verrelli, R.; Black, A. P.; Frontera, C.; Oró-Solé, J.; Arroyo-de Dompablo, M. E.; Fuertes, A.; Palacín, M. R. On the Study of Ca and Mg Deintercalation from Ternary Tantalum Nitrides. *ACS Omega* **2019**, *4* (5), 8943−8952.
(33) Shannon, R. D.; Prewitt, C. T. Effective Ionic Radii in Oxides and Fluorides. *Acta Crystallogr. B* **1969**, *25* (5), 925−946.
(34) Shannon, R. D. Revised Effective Ionic Radii and Systematic Studies of Interatomic Distances in Halides and Chalcogenides. *Acta Crystallogr., Sect. A* **1976**, *32* (5), 751−767.
(35) Goodenough, J. B.; Hong, H. Y.-P.; Kafalas, J. A. Fast Na^+-Ion Transport in Skeleton Structures. *Mater. Res. Bull.* **1976**, *11* (2), 203−220.
(36) Hong, H. Y.-P. Crystal Structures and Crystal Chemistry in the System $Na_{1+x}Zr_2Si_xP_{3-x}O_{12}$. *Mater. Res. Bull.* **1976**, *11* (2), 173−182.
(37) Wang, J.; Wang, Y.; Seo, D.-H.; Shi, T.; Chen, S.; Tian, Y.; Kim, H.; Ceder, G. A High-Energy NASICON-Type Cathode Material for Na-Ion Batteries. *Adv. Energy Mater.* **2020**, *10* (10), 1903968.
(38) Singh, B.; Wang, Z.; Park, S.; Gautam, G. S.; Chotard, J.-N.; Croguennec, L.; Carlier, D.; Cheetham, A. K.; Masquelier, C.; Canepa, P. A Chemical Map of NaSICON Electrode Materials for Sodium-Ion Batteries. *J. Mater. Chem. A* **2021**, *9* (1), 281−292.
(39) Rajagopalan, R.; Chen, B.; Zhang, Z.; Wu, X.-L.; Du, Y.; Huang, Y.; Li, B.; Zong, Y.; Wang, J.; Nam, G.-H.; Sindoro, M.; Dou, S. X.; Liu, H. K.; Zhang, H. Improved Reversibility of Fe^{3+}/Fe^{4+} Redox Couple in Sodium Super Ion Conductor Type $Na_3Fe_2(PO_4)_3$ for Sodium-Ion Batteries. *Adv. Mater.* **2017**, *29* (12), 1605694.
(40) Kawai, K.; Zhao, W.; Nishimura, S.; Yamada, A. High-Voltage Cr^{4+}/Cr^{3+} Redox Couple in Polyanion Compounds. *ACS Appl. Energy Mater.* **2018**, *1* (3), 928−931.
(41) Yabuuchi, N.; Kubota, K.; Dahbi, M.; Komaba, S. Research Development on Sodium-Ion Batteries. *Chem. Rev.* **2014**, *114* (23), 11636−11682.
(42) Wang, Z.; Park, S.; Deng, Z.; Carlier, D.; Chotard, J.-N.; Croguennec, L.; Sai Gautam, G.; Cheetham, A. K.; Masquelier, C.; Canepa, P. Phase Stability and Sodium-Vacancy Orderings in a NaSICON Electrode. *J. Mater. Chem. A* **2021**, *10* (1), 209−217.
(43) Kim, S.; Yin, L.; Lee, M. H.; Parajuli, P.; Blanc, L.; Fister, T. T.; Park, H.; Kwon, B. J.; Ingram, B. J.; Zapol, P.; Klie, R. F.; Kang, K.; Nazar, L. F.; Lapidus, S. H.; Vaughey, J. T. High-Voltage Phosphate Cathodes for Rechargeable Ca-Ion Batteries. *ACS Energy Lett.* **2020**, *5* (10), 3203−3211.
(44) Deng, Z.; Sai Gautam, G.; Kolli, S. K.; Chotard, J.-N.; Cheetham, A. K.; Masquelier, C.; Canepa, P. Phase Behavior in Rhombohedral NaSiCON Electrolytes and Electrodes. *Chem. Mater.* **2020**, *32* (18), 7908−7920.
(45) Kresse, G.; Furthmüller, J. Efficiency of Ab-Initio Total Energy Calculations for Metals and Semiconductors Using a Plane-Wave Basis Set. *Comput. Mater. Sci.* **1996**, *6* (1), 15−50.
(46) Kresse, G.; Furthmüller, J. Efficient Iterative Schemes for Ab Initio Total-Energy Calculations Using a Plane-Wave Basis Set. *Phys. Rev. B* **1996**, *54* (16), 11169−11186.
(47) Kresse, G.; Joubert, D. From Ultrasoft Pseudopotentials to the Projector Augmented-Wave Method. *Phys. Rev. B* **1999**, *59* (3), 1758−1775.
(48) Blöchl, P. E. Projector Augmented-Wave Method. *Phys. Rev. B* **1994**, *50* (24), 17953−17979.
(49) Sai Gautam, G.; Carter, E. A. Evaluating Transition Metal Oxides within DFT-SCAN and SCAN+*U* Frameworks for Solar Thermochemical Applications. *Phys. Rev. Mater.* **2018**, *2* (9), 095401.
(50) Long, O. Y.; Sai Gautam, G.; Carter, E. A. Evaluating Optimal *U* for 3*d* Transition-Metal Oxides within the SCAN+*U* Framework. *Phys. Rev. Mater.* **2020**, *4* (4), 045401.
(51) Sun, J.; Ruzsinszky, A.; Perdew, J. P. Strongly Constrained and Appropriately Normed Semilocal Density Functional. *Phys. Rev. Lett.* **2015**, *115* (3), 036402.
(52) Dudarev, S. L.; Botton, G. A.; Savrasov, S. Y.; Humphreys, C. J.; Sutton, A. P. Electron-Energy-Loss Spectra and the Structural Stability of Nickel Oxide: An LSDA+*U* Study. *Phys. Rev. B* **1998**, *57* (3), 1505−1509.
(53) Anisimov, V. I.; Zaanen, J.; Andersen, O. K. Band Theory and Mott Insulators: Hubbard *U* Instead of Stoner I. *Phys. Rev. B* **1991**, *44* (3), 943−954.

https://doi.org/10.1021/acs.chemmater.2c02841
Chem. Mater. 2022, 34, 10133−10143

(54) Monkhorst, H. J.; Pack, J. D. Special Points for Brillouin-Zone Integrations. *Phys. Rev. B* **1976**, *13* (12), 5188−5192.
(55) Qui, D. T.; Capponi, J. J.; Joubert, J. C.; Shannon, R. D. Crystal Structure and Ionic Conductivity in $Na_4Zr_2Si_3O_{12}$. *J. Solid State Chem.* **1981**, *39* (2), 219−229.
(56) Ong, S. P.; Richards, W. D.; Jain, A.; Hautier, G.; Kocher, M.; Cholia, S.; Gunter, D.; Chevrier, V. L.; Persson, K. A.; Ceder, G. Python Materials Genomics (Pymatgen): A Robust, Open-Source Python Library for Materials Analysis. *Comput. Mater. Sci.* **2013**, *68*, 314−319.
(57) Hart, G. L. W.; Forcade, R. W. Algorithm for Generating Derivative Structures. *Phys. Rev. B* **2008**, *77* (22), 224115.
(58) Hart, G. L. W.; Forcade, R. W. Generating Derivative Structures from Multilattices: Algorithm and Application to Hcp Alloys. *Phys. Rev. B* **2009**, *80* (1), 014120.
(59) Hart, G. L. W.; Nelson, L. J.; Forcade, R. W. Generating Derivative Structures at a Fixed Concentration. *Comput. Mater. Sci.* **2012**, *59*, 101−107.
(60) Morgan, W. S.; Hart, G. L. W.; Forcade, R. W. Generating Derivative Superstructures for Systems with High Configurational Freedom. *Comput. Mater. Sci.* **2017**, *136*, 144−149.
(61) Aydinol, M. K.; Kohan, A. F.; Ceder, G.; Cho, K.; Joannopoulos, J. Ab Initio Study of Lithium Intercalation in Metal Oxides and Metal Dichalcogenides. *Phys. Rev. B* **1997**, *56* (3), 1354−1365.
(62) Hellenbrandt, M. The Inorganic Crystal Structure Database (ICSD)—Present and Future. *Crystallogr. Rev.* **2004**, *10* (1), 17−22.
(63) https://github.com/sai-mat-group/ca-nasicon-electrodes.
(64) Gautam, G. S.; Canepa, P. CHAPTER 4:Theoretical Modelling of Multivalent Ions in Inorganic Hosts. *Magnesium Batteries* **2019**, 79−113.
(65) Sai Gautam, G.; Stechel, E. B.; Carter, E. A. Exploring Ca−Ce−M−O (M = 3*d* Transition Metal) Oxide Perovskites for Solar Thermochemical Applications. *Chem. Mater.* **2020**, *32* (23), 9964−9982.
(66) Sun, W.; Dacek, S. T.; Ong, S. P.; Hautier, G.; Jain, A.; Richards, W. D.; Gamst, A. C.; Persson, K. A.; Ceder, G. The Thermodynamic Scale of Inorganic Crystalline Metastability. *Sci. Adv.* **2016**, *2* (11), e1600225.
(67) Henkelman, G.; Uberuaga, B. P.; Jónsson, H. A Climbing Image Nudged Elastic Band Method for Finding Saddle Points and Minimum Energy Paths. *J. Chem. Phys.* **2000**, *113* (22), 9901−9904.
(68) Rong, Z.; Malik, R.; Canepa, P.; Sai Gautam, G.; Liu, M.; Jain, A.; Persson, K.; Ceder, G. Materials Design Rules for Multivalent Ion Mobility in Intercalation Structures. *Chem. Mater.* **2015**, *27* (17), 6016−6021.
(69) Gao, Y.; Mishra, T. P.; Bo, S.-H.; Sai Gautam, G.; Canepa, P. Design and Characterization of Host Frameworks for Facile Magnesium Transport. *Annu. Rev. Mater. Res.* **2022**, *52* (1), 129−158.
(70) Liu, J.; Wang, S.; Kawazoe, Y.; Sun, Q. Mechanisms of Ionic Diffusion and Stability of the $Na_4MnCr(PO_4)_3$ Cathode. *ACS Mater. Lett.* **2022**, *4* (5), 860−867.
(71) Deng, Z.; Mishra, T. P.; Mahayoni, E.; Ma, Q.; Tieu, A. J. K.; Guillon, O.; Chotard, J.-N.; Seznec, V.; Cheetham, A. K.; Masquelier, C.; Gautam, G. S.; Canepa, P. Fundamental Investigations on the Sodium-Ion Transport Properties of Mixed Polyanion Solid-State Battery Electrolytes. *Nat. Commun.* **2022**, *13* (1), 4470.
(72) Chen, T.; Sai Gautam, G.; Canepa, P. Ionic Transport in Potential Coating Materials for Mg Batteries. *Chem. Mater.* **2019**, *31* (19), 8087−8099.
(73) Perdew, J. P.; Burke, K.; Ernzerhof, M. Generalized Gradient Approximation Made Simple. *Phys. Rev. Lett.* **1996**, *77* (18), 3865−3868.
(74) Devi, R.; Singh, B.; Canepa, P.; Sai Gautam, G. Effect of Exchange-Correlation Functionals on the Estimation of Migration Barriers in Battery Materials. *Npj Comput. Mater.* **2022**, *8* (1), 1−13.
(75) Wexler, R. B.; Gautam, G. S.; Stechel, E. B.; Carter, E. A. Factors Governing Oxygen Vacancy Formation in Oxide Perovskites. *J. Am. Chem. Soc.* **2021**, *143* (33), 13212−13227.
(76) Lide, D. R.*CRC Handbook of Chemistry and Physics*; CRC Press: 2003.
(77) Padhi, A. K.; Nanjundaswamy, K. S.; Goodenough, J. B. Phospho-olivines as Positive-Electrode Materials for Rechargeable Lithium Batteries. *J. Electrochem. Soc.* **1997**, *144* (4), 1188.
(78) Melot, B. C.; Tarascon, J.-M. Design and Preparation of Materials for Advanced Electrochemical Storage. *Acc. Chem. Res.* **2013**, *46* (5), 1226−1238.
(79) Jeon, B.; Heo, J. W.; Hyoung, J.; Kwak, H. H.; Lee, D. M.; Hong, S.-T. Reversible Calcium-Ion Insertion in NASICON-Type $NaV_2(PO_4)_3$. *Chem. Mater.* **2020**, *32* (20), 8772−8780.
(80) Shupack, S. I. The Chemistry of Chromium and Some Resulting Analytical Problems. *Environ. Health Perspect.* **1991**, *92*, 7−11.
(81) Vargas, R.; Galván, M. On the Stability of Half-Filled Shells. *J. Phys. Chem.* **1996**, *100* (35), 14651−14654.
(82) Ponrouch, A.; Palacin, M. R. On the Road toward Calcium-Based Batteries. *Curr. Opin. Electrochem.* **2018**, *9*, 1−7.
(83) Senguttuvan, P.; Rousse, G.; Vezin, H.; Tarascon, J.-M.; Palacín, M. R. Titanium(III) Sulfate as New Negative Electrode for Sodium-Ion Batteries. *Chem. Mater.* **2013**, *25* (12), 2391−2393.
(84) Atkinson, T. D.; Fjellvåg, H.; Kjekshus, A. Synthesis, Structure, and Properties of Chromium(III) Sulfates. *J. Solid State Chem.* **2004**, *177* (11), 4351−4358.
(85) Rentzeperis, P. J.; Christidis, P. C. The crystal structure of rhombohedral $Fe_2(SO_4)_3$. *Z. Für Krist. - Cryst. Mater.* **1976**, *144* (1−6), 341−352.
(86) Hannah, D. C.; Sai Gautam, G.; Canepa, P.; Ceder, G. On the Balance of Intercalation and Conversion Reactions in Battery Cathodes. *Adv. Energy Mater.* **2018**, *8* (20), 1800379.
(87) Amatucci, G. G.; Tarascon, J. M.; Klein, L. C. CoO_2, The End Member of the Li_x CoO_2 Solid Solution. *J. Electrochem. Soc.* **1996**, *143* (3), 1114.
(88) Malik, R.; Abdellahi, A.; Ceder, G. A Critical Review of the Li Insertion Mechanisms in $LiFePO_4$ Electrodes. *J. Electrochem. Soc.* **2013**, *160* (5), A3179.
(89) Sai Gautam, G.; Canepa, P.; Abdellahi, A.; Urban, A.; Malik, R.; Ceder, G. The Intercalation Phase Diagram of Mg in V_2O_5 from First-Principles. *Chem. Mater.* **2015**, *27* (10), 3733−3742.
(90) Aurbach, D.; Lu, Z.; Schechter, A.; Gofer, Y.; Gizbar, H.; Turgeman, R.; Cohen, Y.; Moshkovich, M.; Levi, E. Prototype Systems for Rechargeable Magnesium Batteries. *Nature* **2000**, *407* (6805), 724−727.
(91) Zhou, W.; Xue, L.; Lü, X.; Gao, H.; Li, Y.; Xin, S.; Fu, G.; Cui, Z.; Zhu, Y.; Goodenough, J. B. $Na_xMV(PO_4)_3$ (M = Mn, Fe, Ni) Structure and Properties for Sodium Extraction. *Nano Lett.* **2016**, *16* (12), 7836−7841.
(92) Chen, R.; Butenko, D. S.; Li, S.; Li, D.; Zhang, X.; Cao, J.; Ogorodnyk, I. V.; Klyui, N. I.; Han, W.; Zatovsky, I. V. Effects of Low Doping on the Improvement of Cathode Materials $Na_{3+x}V_{2-x}M_x(PO_4)_3$ (M = Co^{2+}, Cu^{2+}; x = 0.01−0.05) for SIBs. *J. Mater. Chem. A* **2021**, *9* (32), 17380−17389.
(93) Park, S.; Chotard, J.-N.; Carlier, D.; Moog, I.; Duttine, M.; Fauth, F.; Iadecola, A.; Croguennec, L.; Masquelier, C. An Asymmetric Sodium Extraction/Insertion Mechanism for the Fe/V-Mixed NASICON $Na_4FeV(PO_4)_3$. *Chem. Mater.* **2022**, *34* (9), 4142−4152.
(94) Gao, H.; Seymour, I. D.; Xin, S.; Xue, L.; Henkelman, G.; Goodenough, J. B. $Na_3MnZr(PO_4)_3$: A High-Voltage Cathode for Sodium Batteries. *J. Am. Chem. Soc.* **2018**, *140* (51), 18192−18199.
(95) Long, O. Y.; Sai Gautam, G.; Carter, E. A. Assessing Cathode Property Prediction via Exchange-Correlation Functionals with and without Long-Range Dispersion Corrections. *Phys. Chem. Chem. Phys.* **2021**, *23* (43), 24726−24737.
(96) Richardson, I. G. The Calcium Silicate Hydrates. *Cem. Concr. Res.* **2008**, *38* (2), 137−158.